Journal of Non-Crystalline Solids 465 (2017) 8–16

Contents lists available at ScienceDirect

Journal of Non-Crystalline Solids

journal homepage: www.elsevier.com/locate/jnoncrysol

Nanoindentation investigation on creep behavior of amorphous Cu—Zr—Al/nanocrystalline Cu nanolaminates

Y. Ma [a], G.J. Peng [a], Y.H. Feng [b], T.H. Zhang [a,*]

[a] Institution of Micro/Nano-Mechanical Testing Technology & Application, College of Mechanical Engineering, Zhejiang University of Technology, Hangzhou 310014, PR China
[b] State Key Laboratory of Nonlinear Mechanics (LNM), Institute of Mechanics, Chinese Academy of Sciences, Beijing 100190, China

ARTICLE INFO

Article history:
Received 8 February 2017
Received in revised form 23 March 2017
Accepted 26 March 2017
Available online 2 April 2017

Keywords:
Nanolaminates
Amorphous alloy
Nanoindentation
Creep
Strain rate sensitivity

ABSTRACT

Berkovich nanoindentation experiments have been performed on amorphous /nanocrystalline nanolaminates with individual Cu—Zr—Al layers (45 nm, 90 nm, 225 nm) and Cu layers (7.5 nm & 15 nm). Elastic modulus, hardness and indentation morphology were detected and compared to those of single Cu—Zr—Al thin film. Creep deformation was systematically investigated at various holding depths and loading rates. For the sample with thinner amorphous layer, a more pronounced creep deformation was observed and it was confirmed to be due to the size effect of Cu—Zr—Al layers and the addition of Cu layers. The creep deformation was identified to be history-independent through applying various loading rates. The strain rate sensitivities were calculated from the steady-state creep and a sharp enlargement appeared as the amorphous layer reduced down to 90 nm, implying a transition of creep mechanism in nanolaminates.

1. Introduction

As a relatively new member of glass family, amorphous alloy has a great potential to be utilized as engineering material for excellent mechanical properties, such as large elastic limit, high strength and strong wear resistance [1]. However, the limited size and limited plasticity are currently the two critical bottlenecks hinder the development of amorphous alloy for commercial applications. Tremendous research efforts have been performed on developing new compositions and amorphous alloy-based composites in past years [2–4]. Introducing crystalline phases has been proved to be an effective way to improve the ductility of amorphous alloy and without sacrificing their high strength [4]. Amorphous/Crystalline (A/C) nanolaminates are intensively studied due to the simple preparation, controllable components and application feasibility. Wang et al. [5] reported a high flow stress of 1.09 GPa combined with a tensile elongation up to 13.8% in a A/C nanolaminate with individual 5 nm Cu—Zr layers. In Kim et al.'s work [6], the maximum strength and plastic strain at failure for the nanolaminate with 112 nm Cu—Zr and 16 nm Cu layers reached up to 2.513 GPa and 4%, respectively. In recent years, people performed nanoindentation tests on A/C nanolaminates in order to reveal the underlying deformation mechanism [7–9], including the interface effect [10], deformation-induced devitrification [11], size effect [12] and chemical mixing [13]. Intrinsically, the ductile phase suppresses the propagation of shear bands (or STZs) rather than changing the deformation mechanism of amorphous alloys. Therefore it also opens a new train of thought for studying the size effect of amorphous alloys on plastic deformation experimentally in A/C nanolaminates, especially below100 nm [6,7,9,12].

Creep resistance has been of great importance and interest from both technological and scientific points of view. Nanoindentation is the most powerful technology to study the mechanical properties of small-sized samples. Meanwhile the holding stage could be efficient in nanoindentation due to the high accuracy for obtaining the creep flow [14]. Therefore it was widely employed to investigate the room-temperature creep deformation of thin film [15], nanopillar [16] as well as crystalline-crystalline nanolaminates [17]. To the authors' best knowledge, creep behaviors of A/C nanolaminates have not been reported yet and far from understanding. With this in mind, nanolaminates consisting of amorphous Cu—Zr—Al layers and nanocrystalline Cu layers were fabricated and their mechanical properties were measured by nanoindentation. In the present work, we aim to explore the creep behavior of A/C nanolaminate and its correlation with individual layer thickness, holding depth and loading rate. The indentation experiments were also conducted in single Cu—Zr—Al thin film as a comparison.

2. Experimental procedures

The amorphous Cu—Zr—Al film and Cu—Zr—Al/Cu nanolaminates were deposited on silicon wafer in a RF magnetron sputtering system (Kurt J. Lesker PVD75) at room temperature in pure argon gas. The 2-in. target alloys adopt in the chamber are $Cu_{45}Zr_{48}Al_7$ (at.%) and pure Cu which were prepared from high purity (99.99%) elements by vacuum casting. The target was installed at the bottom while the silicon

* Corresponding author.
E-mail address: zhangth@zjut.edu.cn (T.H. Zhang).

http://dx.doi.org/10.1016/j.jnoncrysol.2017.03.037
0022-3093/

wafer was stick on the sample platform, which is right above the target. The target-to-substrate distance is kept constant, equal to 100 mm. The base pressure of the chamber was kept at about $4 * 10^{-7}$ Torr before deposition and working argon pressure was set to about 1mTorr. The power on the targets was fixed at 150 W for Cu—Zr—Al target and 80 W for Cu target. Film thickness could be accurately controlled by setting working time. Five kinds of nanolaminates with different layer thickness were prepared, namely, 50 nm amorphous Cu—Zr—Al/20 nm nc Cu, 100 nm amorphous Cu—Zr—Al/20 nm nc Cu, 250 nm amorphous Cu—Zr—Al/20 nm nc Cu and 50 nm amorphous Cu—Zr—Al/10 nm nc Cu, 250 nm amorphous Cu—Zr—Al/10 nm nc Cu. The top and bottom layers in the nanolaminates are both Cu—Zr—Al. The film thickness was measured by a surface profilometer (Dektak 150), and the layer thickness was confirmed from the film cross-section by scanning electron microscope (SEM) (MOI-ZEISS). Here the total film thickness is about 1600 nm. The structures of the samples were detected by X-ray diffraction with Cu K_α radiation. By means of X-ray energy dispersive spectrometer (EDS) attached on the SEM, chemical composition of the amorphous film was detected as $Cu_{44}Zr_{44}Al_{12}$.

Nanoindentation experiments were conducted at constant temperature of 20 °C on Agilent Nano Indenter G200 with a standard Berkovich indenter. Prior to the creep testing, hardness and elastic modulus were measured through continuous stiffness measurement (CSM) technique at a constant strain rate of 0.05 s^{-1}. Scanning probe microscopy (SPM) and atomic force microscopy (AFM) (OLYMPUS, OLS4500) were used to examine the surface roughness and nanoindentation morphologies, in which the maximum displacement is 1000 nm and strain rate is 0.05 s^{-1}. The constant-load holding method was used in this work to explore the creep behaviors. The indenter was held for 250 s at a series of loading-unloading cycles with different maximum depths of 50 nm, 100 nm, 150 nm and 200 nm. In these cases, the loading strain rate was fixed, equal to 0.05 s^{-1}. Furthermore, the influence of loading rate on the creep behavior was studied at a maximum load of 5 mN. Four different loading rates of 0.05 mN/s, 0.1 mN/s, 0.5 mN/s and 2.5 mN/s were employed. The creep tests were carried out until thermal drift reduced to below 0.02 nm/s. Meanwhile, drift correction which was calibrated at 10% of the maximum load during the unloading process would be strictly performed. To ensure the reliability of creep results, measurements in groups of twelve were conducted for each case.

3. Results and discussion

3.1. Structure, elastic modulus and hardness

Fig. 1(a) shows the typical X-ray diffraction patterns of the as-prepared Cu—Zr—Al film and Cu—Zr—Al/Cu nanolaminates. It is clear that only a broad diffraction peak can be detected in pure Cu—Zr—Al sample, which represents a crystal-free structure. The intensities of Cu (111) and Cu (200) peaks enhanced with the increase of Cu content in the compounds. The cross section morphologies of the nanolaminates were shown in Fig.1 (b)–(f). The effective thickness of individual Cu—Zr—Al layer was measured as 45 ± 0.8 nm, 90 nm ± 1.3 and 225 ± 1.8 nm, which were linearly increased with depositing time. Due to the limited accuracy of SEM observation, the thickness of individual Cu layer could be estimated by $l = \frac{T-n^*L}{n-1}$, in which T is the total film thickness, n is the number of Cu—Zr—Al layer and L is the thickness of individual Cu-Zr-Al layer. The two kinds of Cu layers are actually 15 nm and 7.5 nm on average. The nanolaminates are referred to as A45C7.5, A225C7.5, A45C15, A90C15 and A225C15. As an illustration, A45C15 is used to denote the sample contains alternating 45 nm amorphous layers and 15 nm crystalline layers.

Fig. 2 shows the elastic modulus E_{-IT} and hardness H as a function of indentation depth for the A90C15 sample as an illustration, in which eight effective CSM indents were selected. The experimental performance exhibits a good reliability once the pressed depth beyond about 100 nm. The disparities of elastic modulus and hardness at shallow depth were mainly due to the tip imperfection. The elastic modulus and hardness were obtained at the displacement of 200 nm for all the samples, as listed in Table.1. The elastic modulus was slightly increased with increasing Cu content in the sample. It is widely accepted that the elastic modulus is sample size-independent for a material. The elastic modulus of Cu film approximately lies between 120 GPa and 190 GPa [18], which is higher than amorphous Cu—Zr—Al. According to the

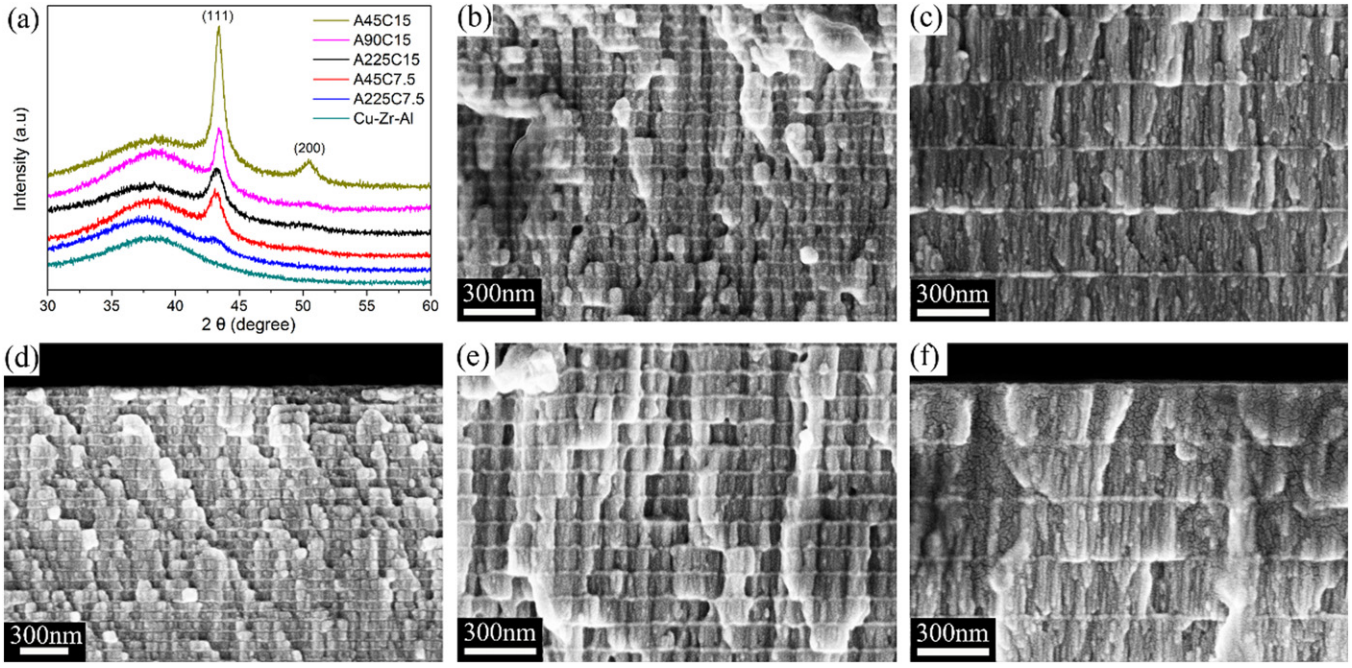

Fig. 1. (a) Typical XRD patterns of the Cu-Zr-Al film and Cu-Zr-Al/Cu nanolaminates; Cross-section micrographs of the (b) A45C7.5, (c) A225C7.5, (d) A45C15, (e) A90C15 and (f) A225C15 nanolaminates by SEM.

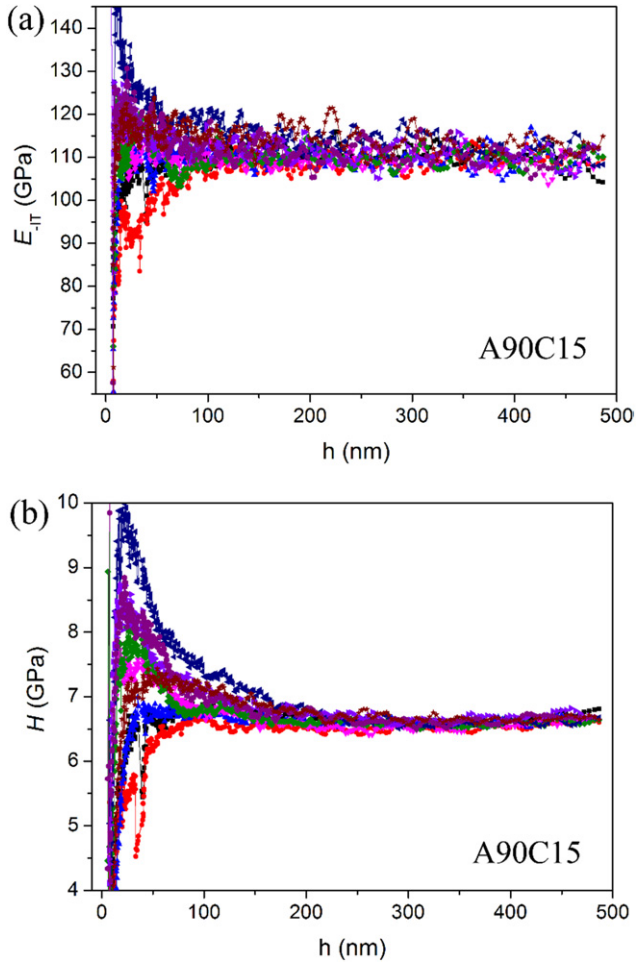

Fig. 2. (a) Elastic modulus and (b) hardness as a function of indentation depth by CSM for the A90C15 sample.

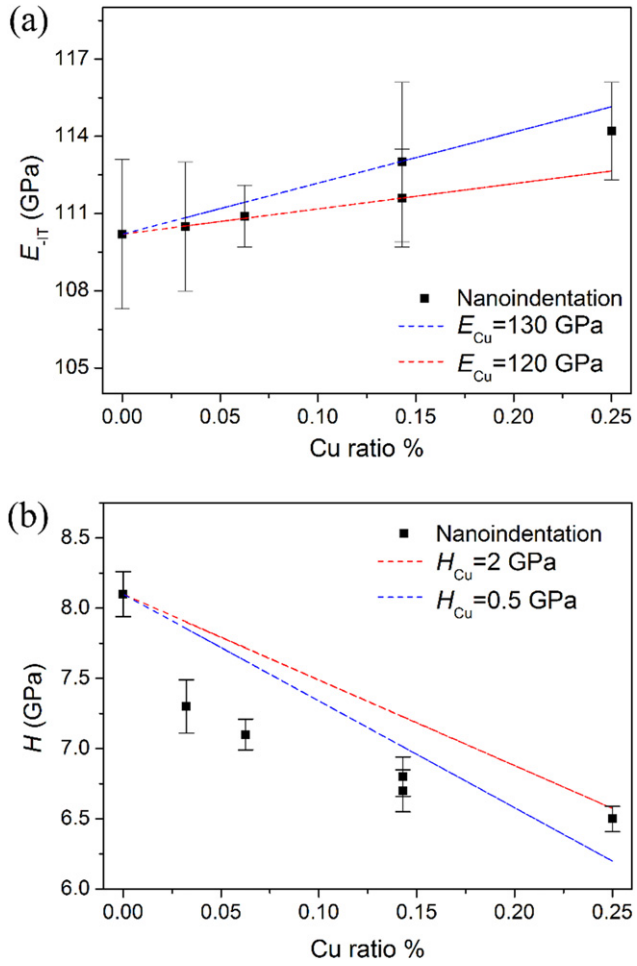

Fig. 3. (a) Elastic modulus and (b) hardness with standard deviations by nanoindentation CSM as a function of Cu content for all the samples. Isostrain predictions upon the rule of mixture were also shown. (Suppose E & H are unchanged with layer thickness in both Cu-Zr-Al and Cu).

rule of mixture, it is reasonable to have higher elastic modulus in the nanolaminates with more Cu layers. Fig. 3(a) shows the elastic modulus as a function of Cu content in the samples. The nanoindentation data fall within the theoretical bounds, in which E_{Cu} = 120 GPa and E_{Cu} = 130 GPa were adopted as lower and upper boundaries for Cu layer. It is worth noting that the measured elastic modulus of nanolaminates would be influenced by the presence of interfacial stress. Due to the approached values of elastic modulus for the amorphous Cu—Zr—Al and Cu layers, the interfacial effect would be negligible here.

On the other hand, hardness (or strength) is strongly correlated with both the physical and structural size in crystalline metals [19] though it is controversial that whether such size effect exists in amorphous alloys [20]. It has been reported the flow strength of nanocrystalline Cu distributed in a large range [21]. We roughly adopted 200 MPa and 800 MPa as the minimum and maximum values to estimate the strength of Cu layer herein. Based on the mode of Tabor, hardness can be related with flow strength via $H = \alpha\sigma_f$, and α was set to be 2.5 for simplicity [22]. Provided that the hardness of Cu—Zr—Al kept constant with various thicknesses, the variation trend of hardness in nanolaminates was apparently disobeyed the rule of mixture, as shown in Fig. 3(b). Presumably, this could be explained through both computation error and intrinsic structure change. The morphology of pile-up always arises during indentation in hard metals such as amorphous alloys [9], which leads to a smaller contact displacement in record and hence a higher value of hardness. This can be substantially confirmed from the lateral profiles of Cu—Zr—Al film by SPM technology, as shown in Fig. 4(a). With the addition of Cu layers in Fig. 4(b)–(d), the degree of pile-up height was gradually alleviated. Thus the nominal hardness dropped more than the estimation by rule of mixture. Besides, more content of Cu was suffered from yield stress beneath the indenter than it was expected in calculation. The hardness would be overestimated for the nanolaminates by the rule of mixture relying on the nominal ratio of Cu content. On the other side, the plastic deformation manner of single Cu—Zr—Al film would be largely different from the A/C nanolaminates. Fig. 4 also shows the nanoindentation AFM morphologies for the four samples. Abundant large-sized shear offsets were appeared in Cu—Zr—Al film while very limited ones were observed in A225C15 and A90C15 samples, and finally disappeared in A45C15 sample. It indicates that the localized deformation was suppressed as the amorphous layer reduced form micrometer scale to ten of nanometers, which

Table 1
Elastic modulus and hardness by CSM for all the samples.

Sample	Cu—Zr—Al	A225C15	A90C15	A45C15	A225C7.5	A45C7.5
E_{-IT}, GPa	110.2 ± 2.9	110.9 ± 1.2	111.6 ± 1.9	114.2 ± 1.9	110.5 ± 2.5	113.0 ± 3.1
H, GPa	8.1 ± 0.16	7.2 ± 0.11	6.7 ± 0.15	6.5 ± 0.09	7.3 ± 0.19	6.8 ± 0.14

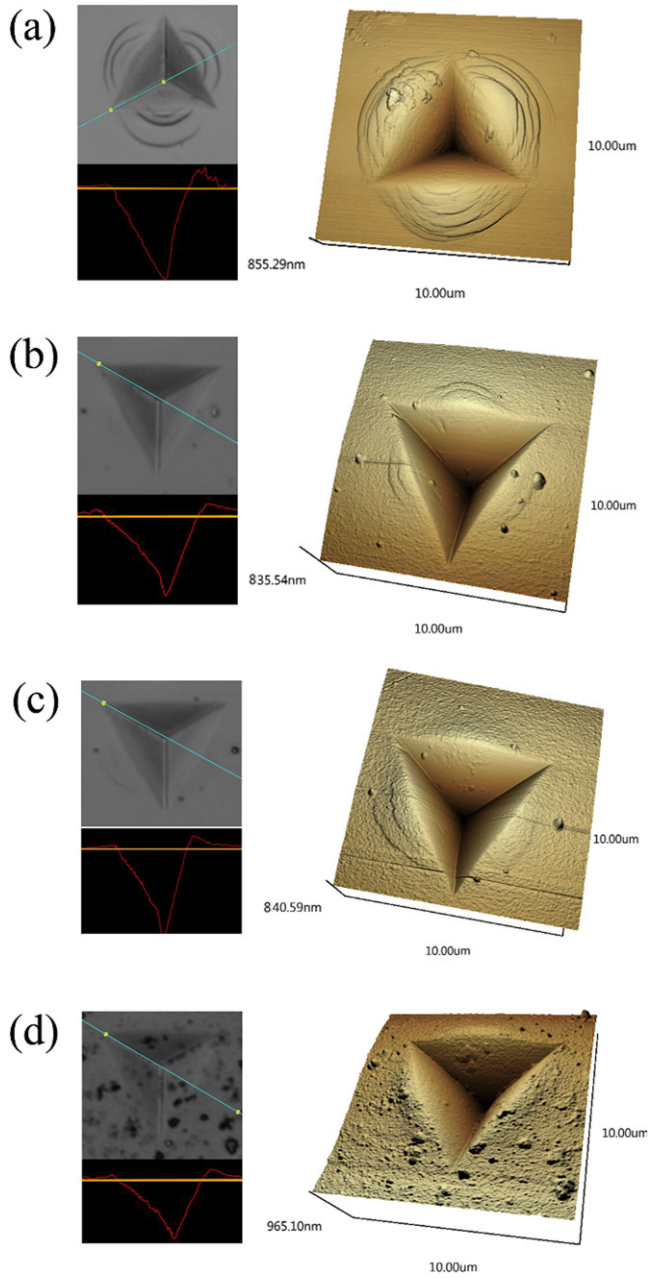

Fig. 4. Representative nanoindentation SPM and AFM images of (a) Cu-Zr-Al, (b) A225C15, (c) A90C15 and (d) A45C15 samples, showing the degree of pile-up and nanoindentation morphologies.

could be due to the restriction for shear banding propagation in narrow space [23]. And the strength of amorphous layer could be increased as thickness reducing [6]. It should also be mentioned that both the blocking effect of Cu layer [7] and strengthen effect of chemical mixing [13] would be considerable on the mechanical response in A45C15, further increasing the hardness of nanolaminates. These may explain why the hardness of A45C15 approached to the upper bound of theoretical value in Fig. 3(b).

3.2. Creep behaviors

Fig.5 shows the typical creep deformations with various initial holding depths, which were plotted with holding time. In order to recognize the effect of holding depth on creep behavior more intuitively, the starting points (including both the holding time and creep displacement) for all the creep curves were set to be zero. For the Cu—Zr—Al, A225C15, A90C15 and A45C15 samples, the creep deformation clearly occurred and was enhanced by increasing initial depth. In previous studies, it was revealed that creep was commonly observed in nanoindentation for many high-melting point materials such as amorphous alloys and high-entropy alloy [15,24–26]. In comparison to the standard creep test, severely plastic deformation has already occurred at the onset of holding stage in nanoindentation. Therefore the indentation creep would be an expanding progress of the plastic zone, substantially distinct from the mechanism of elastic holding creep. The indentation creep could be roughly divided into transient stage (0 s–25 s) and steady-state (25 s–250 s) stage here. “strain burst” has been reported in the creep deformation of polycrystalline Cu thin film [27], Cu—Zr—Al—Ag amorphous alloys [28] and Ag/Cu nanolaminates [29]. Such phenomenon was not appeared in the present work.

The total creep displacement Δh was recorded and plotted with the initial holding depth h_0 for all the samples, as shown in Fig. S1. With increasing the initial depth, the creep displacement almost linearly increased in both amorphous film and A/C nanolaminates. Furthermore, the creep displacement was more pronounced in A/C nanolaminate, whilst more precipitously increased with initial depth than that in pure Cu—Zr—A. Fig. 6(a) summarized the average creep displacement with various initial depth in Cu—Zr—Al film and nanolaminates with 15 nm Cu layers for a clear view. Obviously, the thinner amorphous layer the nanolaminate contained, the more pronounced creep deformation occurred. For a standard Berkovich indenter, the imposed plastic strain and stress distribution during testing are self-similar at various penetration depths. The maximum stress and structure mobility would promote creep flow in the plastic region rather than elastic region beneath the indenter. Noticed that the plastic region is proportional to the indenter depth. By this analysis, it's reasonable that creep displacement is larger at deeper location. Notwithstanding the stress distribution is much more complicate beneath the indenter, the creep strain could be expressed as creep displacement versus initial displacement in the Berkovich indentation for simplicity. Fig. 6(b) shows the average indentation creep strain for the samples at various initial depths. Ideally, it should be constant for each sample. However, the creep strain was decreased with increasing the initial depth. This observation could be due to both artificial and intrinsic reasons. At transient creep stage, indentation displacement increases substantially fast and reaches a considerable value in a very short time (~25 s). We can image that apparatus error would play an important role at the very beginning of the holding stage. Though it's hard to quantify the contribution of indenter “overshoot” on the transient creep, the true creep strain would suffer less disturbance at deeper depth. Provided that such indenter “overshoot” is equal at various holding depth (with which loading sequence is the same 0.05 s^{-1}), the creep strain could be rewritten as $\frac{\Delta h}{h_0} - \frac{\Delta h_1}{h_0}$, Δh_1 is the “overshoot” displacement. If we suppose $\Delta h_1 = 1.5$ nm, then the true creep strain was practically at the same level with various holding depths as shown in Fig. 6(c). Besides, it was reported that indentation creep would be affected by the instantaneous plastic deformation at the onset of holding stage [31]. The density of dislocations in crystal or shear bands in amorphous alloys is higher at smaller indentation depth, causing more “fertile” regions and better structure fluidity to promote creep deformation.

The noticeable structural differences among the samples are the thickness of amorphous layer and crystalline Cu content. Cu—Zr—Al thickness and crystalline Cu content are correlative and namely the same variable that the increasement of Cu content is in direct proportion to the decreasement of amorphous layer thickness. The creep displacements of A/C nanolaminates were found to be nearly linearly increased with crystalline Cu content increasing (or Cu—Zr—Al layer thickness reducing), as shown in Fig. 6(d). In accordance with the variation of hardness, the creep resistance was declined in the sample with more Cu content (or thinner Cu—Zr—Al layer). It was reported that indentation creep was easy to occur in Cu films regardless of grain size

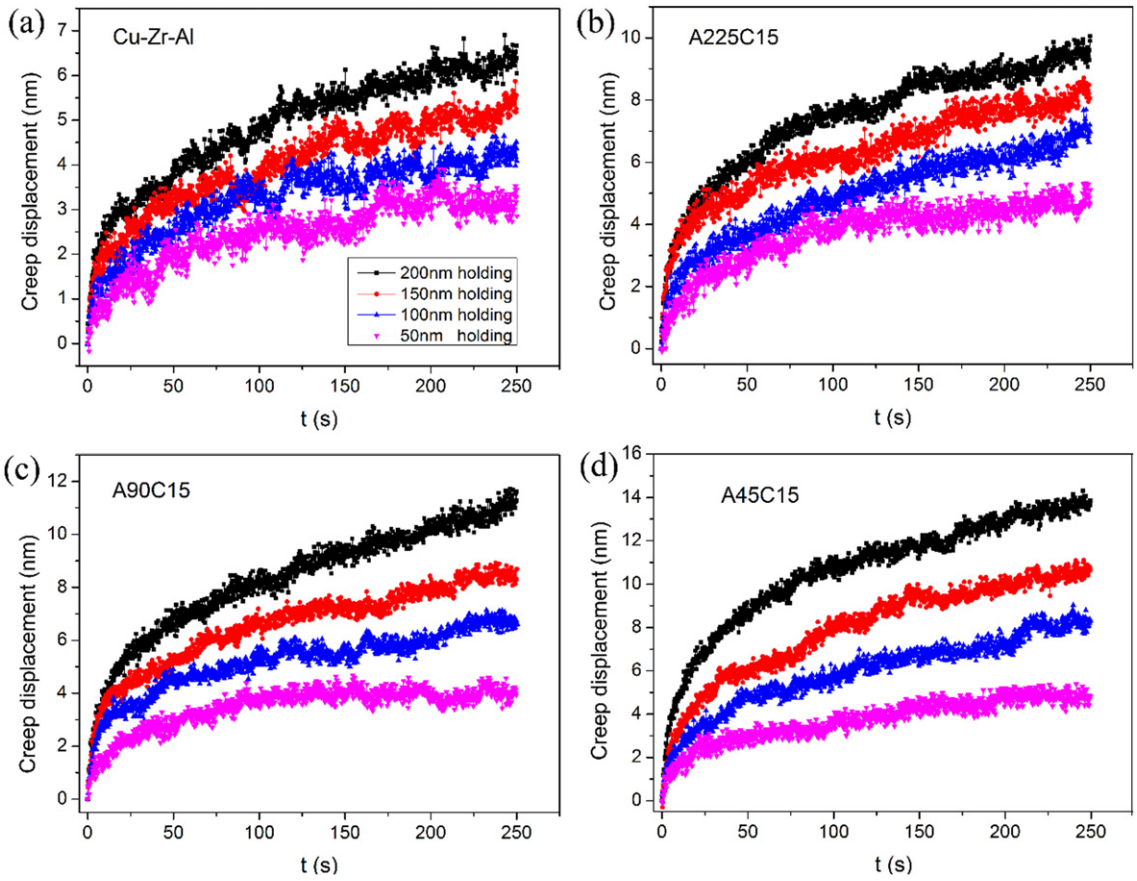

Fig. 5. Typical creep displacements versus holding time at the initial holding depth of 50 nm, 100 nm, 150 nm and 200 nm for (a) Cu-Zr-Al film, (b) A225C15, (c) A90C15 and (d) A45C15 nanolaminates.

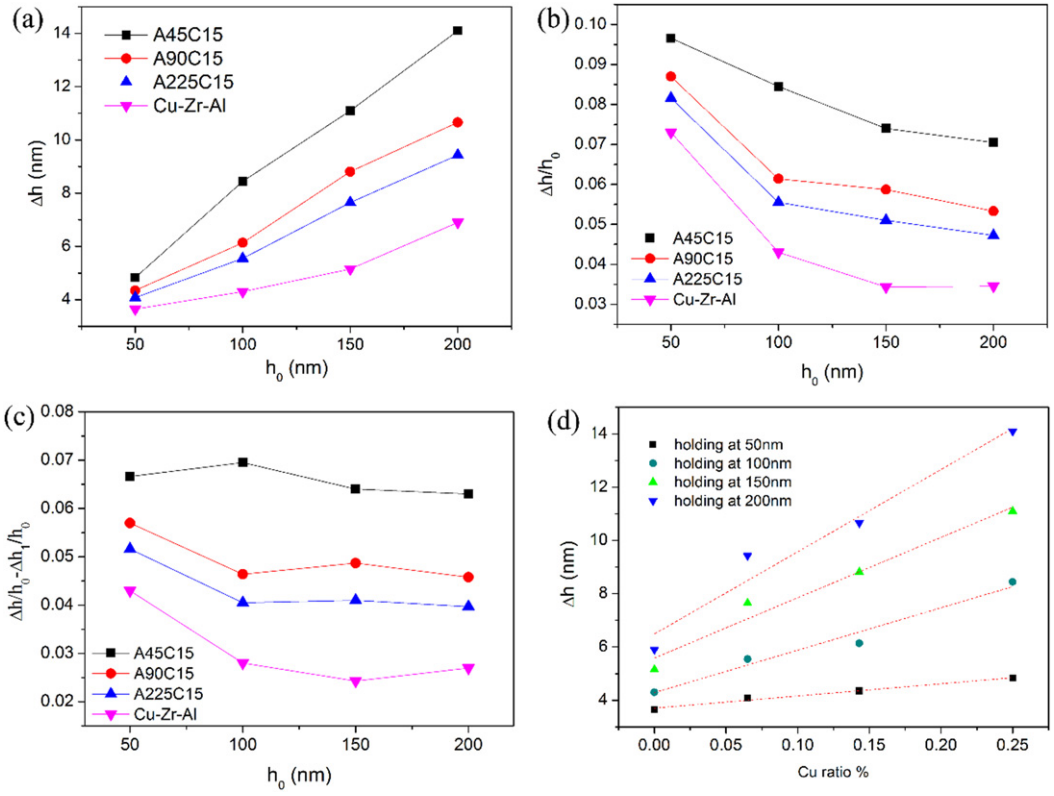

Fig. 6. The averaged (a) total creep displacement and (b) creep strain for all the samples at various initial holding depth h_0; (c) true creep strain by subtracting indenter "overshoot"; (d) the total creep displacement as a function of Cu ration in the samples.

[27,31,32]. While Yoo et al. have revealed that creep behavior in amorphous alloy nanopillars is strongly correlated with the sample size under elastic holding [16]. The authors also reported that creep deformation could be largely enhanced as reducing the thickness of a Cu—Zr—Al thin film from 1500 nm to 500 nm [33]. Notwithstanding the disparities of imposed conditions on nanoindentation, it's suggested that the size reduction of amorphous layer would play an important role on creep enhancement here. Therefore the more pronounced creep deformation could be explained on both effects of thinner amorphous layers and more Cu contents simultaneously.

The creep behaviors of A45C7.5 and A225C7.5 laminates were studied by the same analysis, in order to explore the effect of Cu layer thickness. The total creep displacements at the initial holding depths of 50 nm, 100 nm, 150 nm and 200 nm were summarized respectively, as shown in Fig. S1(e)&(f). Fig. 7(a) shows the mean values of creep displacement for the A45C7.5, A45C15 and A90C15 samples. In comparison to the A45C15 sample, the creep displacements of the A45C7.5 sample were almost the equal at shallow holding depths (50 nm & 100 nm), and were slightly lowered at deep holding depths (150 nm & 200 nm). While the creep displacements of the A45C7.5 sample were apparently higher than those of A90C15 sample at holding depths of 100 nm, 150 nm and 200 nm (artificial error largely reduced the Δh disparity between two samples at 50 nm). Fig. 7(b) shows the mean values of creep displacement for the A225C7.5 and A225C15 samples, between which the maximum gap was less than 1 nm. Noted that the creep displacements of A225C7.5 sample were even increased at 100 nm and 150 nm holdings. The two groups of comparison on creep deformation (A45C15 vs. A45C7.5, A225C15 vs. A225C7.5) indicate that the thickness of Cu layer do not substantially affect creep behavior of A/C nanolaminates. It is implied the creep deformation in 7.5 nm Cu layers was very close to that in 15 nm Cu layers. The comparison between A45C7.5 and A90C15 samples could further confirms that the increased amount of Cu layers (rather than the content of Cu) and the decreased size of amorphous layers are the intrinsic reasons for the creep enhancement.

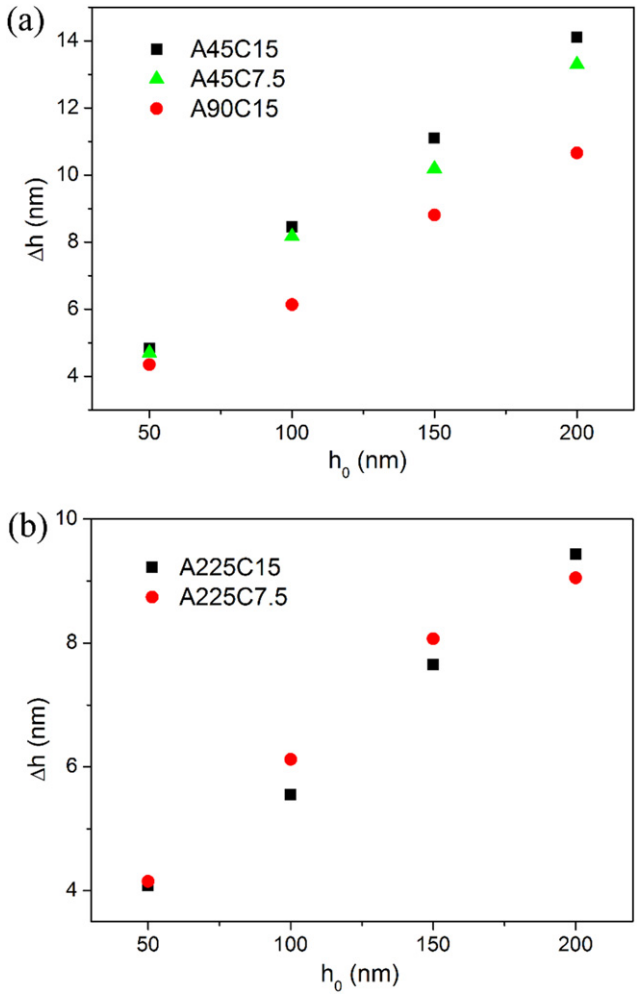

Fig. 7. (a) Comparison of creep displacement among A45C15, A45C7.5 and A90C15 nanolaminates at various initial holding depth h_0. (b) Comparison of creep displacement between A225C15 and A225C7.5 nanolaminates.

3.2.1. Loading rate effect

In the previous reports, higher loading rate facilitates nanoindentation creep in both amorphous alloys and nano-crystalline Cu [31,34,35]. It was reasonable that the plastic mechanisms of both amorphous and crystalline solids are influenced by strain rate, as well as the plastic morphologies beneath the indenter. Consequently, the structure state at the beginning of holding stage could be related with the loading sequence. Furthermore, the holding duration was comparable to the loading time in nanoindentation creep tests. Creep deformation was thought to be "consumed" at the longer loading process, reducing the displacement during the holding stage. For certifying the creep law in Fig. 6, creep tests with various loading rates were conducted under maximum load of 5 mN. Fig. 8 shows the typical load vs. displacement curves for the Cu-Zr-Al film and nanolaminates with loading rates of 2.5 mN/s, 0.5 mN/s, 0.1 mN/s and 0.05 mN/s. The loading curves were almost overlapped in Fig. 8(a), indicating a strain rate-insensitive hardness in Cu—Zr—Al film. This phenomenon is consistent with the low value of strain rate sensitivity (SRS) in amorphous alloys, which was reported commonly in magnitude of 10^{-4}–10^{-3} and sometimes even minus [36]. While the loading sequence is loading rate-dependent in nanolaminates, it is clear that larger indentation depth is required to reach the same load for the slower loading tests, particularly in A45C15. It is understandable that higher positive correlation between hardness and loading rate (or strain rate) was found in the nanolaminates with more Cu content which owns a relative high value of SRS on the magnitude of ~10^{-2} [37]. The corresponding creep displacements versus time are shown in the insets. Notwithstanding the loading rates adopted here spanned two orders of magnitude, the creep curves were almost overlapped for all the samples. It is indicated that the creep deformation was history-independent in both Cu—Zr—Al film and Cu—Zr—Al/Cu nanolaminates. This phenomenon is not contradictory to the aforementioned studies on the correlation between creep deformation and loading rates. The authors have revealed that the loading rate effect on creep deformation is correlated with compositions and intrinsically associated with the shear transformation zone size in amorphous alloys by spherical nanoindentation [34]. The same phenomenon was also observed in a high-entropy alloy with BCC structure by Berkovich nanoindentation [26]. The development of shear bands and/or dislocations would be arrested at the interface between amorphous and nancrystalline layers. Therefore, the blocking effect of interface would alleviate the structure disturbance by different loading rates in A/C laminates.

3.2.2. Strain rate sensitivity

Indentation creep also has been the most extended method to study strain rate sensitivity (SRS) in metals. From indentation-creep tests, SRS for a power-law creeping material can be directly obtained by applying time-displacement data, through the relationship between creep stress and strain rate. The value of SRS exponent m can be evaluated via:

$$m = \frac{\partial \ln \tau}{\partial \ln \dot{\varepsilon}} \quad (1)$$

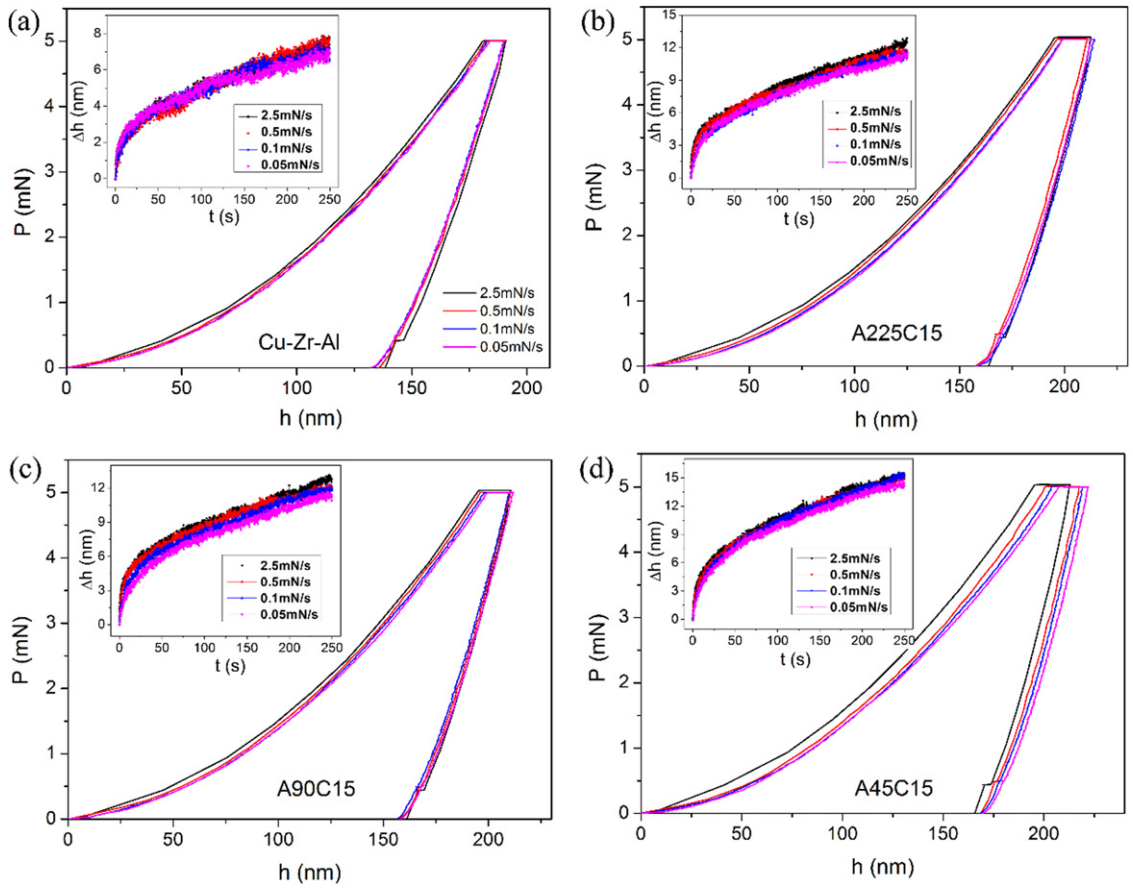

Fig. 8. Representative load-displacement curves with four different loading rates in (a) Cu-Zr-Al, (b) A225C15, (c) A90C15 and (d) A45C15 films. The creep displacements versus holding time are also plotted in the insets for all the samples.

For a standard Berkovich indentation process, the strain rate $\dot{\varepsilon}$ during the holding stage can be calculated as:

$$\dot{\varepsilon} = \frac{dh}{dt_{creep}} \frac{1}{h} \tag{2}$$

Flow stress τ is generally assumed to be ~$H/3$ and nanoindentation hardness is defined as:

$$H = \frac{P}{24.5h_c^2} \tag{3}$$

The plastic displacement h_c could be deduced as $h_c = h - \varepsilon \times P/S$ [38], in which h is the total indentation displacement, $\varepsilon = 0.72$ for a Berkovich tip, S is the stiffness deduced from the unloading curve and increased with pressed depth. In the current study, it's unrealistic to detect S at each recorded creep displacement. For simplicity, the S obtained from the creep unloading curve was adopted to calculate hardness. Here we adopted creep curves at 200 nm holding to estimate the SRS for all the samples.

The experimental data could be perfectly fitted ($R^2 > 0.99$) by an empirical law:

$$h(t) = h_0 + a(t - t_0)^b + kt \tag{4}$$

where h_0, t_0 are the initial displacement and time at the beginning of holding stage. a, b, k are the fitting constants. Fig. 9(a) shows the creep curves and fitting lines in Cu—Zr—Al film and the laminates with 15 nm Cu layer. Fig. 9(b) shows the variation of strain rates as a function of creep time deduced from the fitting lines. The creep strain rates were dropped precipitously from the magnitude of 10^{-2} s^{-1} to 10^{-4} s^{-1} within the initial 50 s, especially for Cu—Zr—Al film. Then it was decreased gently and fall into the range of 10^{-4} s^{-1} to 10^{-5} s^{-1} for all the four samples during the last 100-s duration, as exhibited in the inset of Fig. 9(b). It was also illustrated that the creep strain rate was accelerated with the increasing Cu content among the four samples. Fig. 9(c) shows the variation of "hardness" (denotes stress variation, true hardness is constant here) as a function of creep time. It was reduced from 8.40 GPa to 7.78 GPa for Cu—Zr—Al, 7.0 GPa to 6.33 GPa for A225C15, 6.74 GPa to 5.95 GPa and 6.35 GPa to 5.50 GPa for A45C15 after 250 s holding. The creep stress could be expected to drop down 7.4%, 9.6%, 11.7% and 13.4% for the Cu—Zr—Al, A225C15, A90C15 and A45C15 respectively. Fig. 9(d) shows the logar-logar correlation between indentation hardness and strain rate during the holding stage. SRS can be obtained by linearly fitting the part of steady-state creep. The creep curves of A45C7.5 and A225C7.5 were addressed by the same analogy, as shown in Fig.S2. For reliability, 6–8 effective creep curves were employed to reach an average value of SRS for each sample. The estimated SRSs are 0.021, 0.023, 0.022, 0.033, 0.035 and 0.034 for Cu-Zr-Al, A225C7.5, A225C15, A90C15, A45C7.5 and A45C15 respectively, as exhibited in Fig.10. Here m is in the order of 10^{-2}, which could be due to method characteristic that lower m is always obtained by the rate-jump method [39]. Clearly, a sharp rise of m was observed when the amorphous layer reduced down to 90 nm.

The value of SRS or stress exponent ($n = 1/m$) can indicate creep mechanism in traditional creep testing. Though the nanoindentation creep is apparently mechanical activated and its mechanism would be varied from the traditional results, the change of SRS could also be concerned with the transition of creep manners in A/C nanolaminates. In volkert's work [40], it was revealed that SRS kept constant for

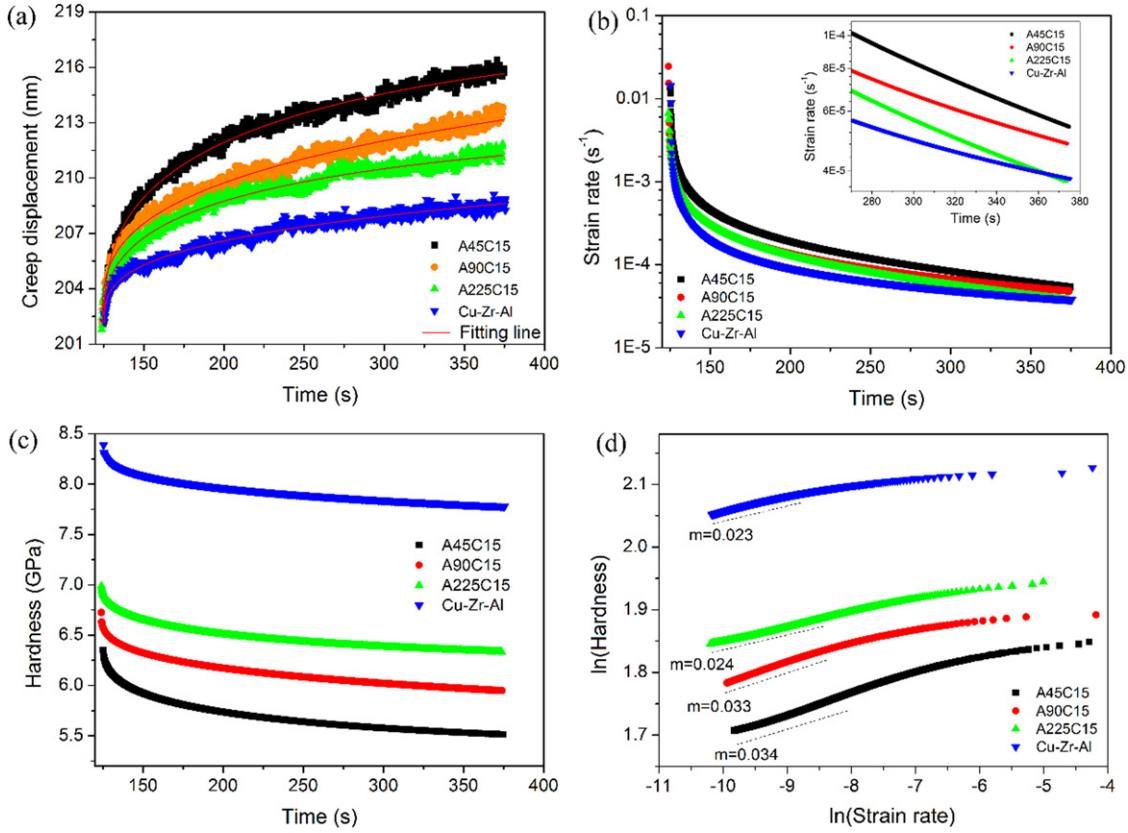

Fig. 9. (a) The typical creep curves and the fitting lines for Cu-Zr-Al and the nanolaminates with 15 nm Cu layers; (b) The creep strain rate as a function of holding time; (c) The creep hardness as a function of holding time; (d) The logar-logar correlation between hardness and strain rate during the creep deformation, strain rate sensitivities can be computed from the steady-state part.

amorphous alloy with various sample sizes at nano-scale. Qualitatively, the Cu layers would play a negligible effect on creep deformation in the sample with 225 nm amorphous layer, which explains the very close values of SRS in Cu—Zr—Al, A225C15 and A225C7.5. For the A90C15 sample, it is reasonable to have a higher SRS due to the participation of Cu layers in creep flow. Despite the more pronounced creep deformation in A45C15 and A45C7.5, their SRSs changed very little from A90C15. It is suggested that the creep enhancement could not be simply due to the reduction of amorphous layer size and/or addition of Cu layers. Otherwise, SRS would increase accordingly with increasing Cu layers. Perhaps interfacial slip played an important role on the creep deformation in these samples, which may causes the creep mechanism more complicated in A/C nanolaminates.

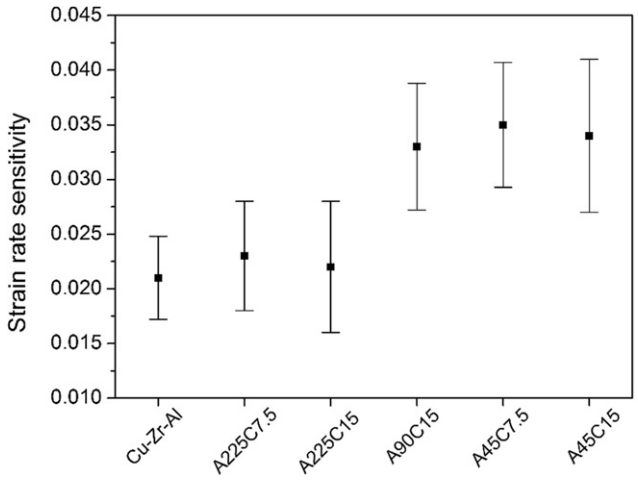

Fig. 10. Strain rate sensitivities deduced from steady-state creep for all the samples.

4. Conclusion

In summary, nanoindentation creep behaviors of nanolaminates with individual amorphous alloy layers and nanocrystalline Cu layers were systematically investigated. The creep displacements were increased with increasing holding depths, while it was revealed the creep strains beneath a Berkovich indenter were actually constant. The experimental results show that the thinner Cu—Zr—Al layer the nanolaminate contains, the more pronounced creep deformation occurs and the underlying reason was discussed. Besides, the creep deformation was found to be history-independent in both amorphous alloy film and nanolaminates. Finally, the strain rate sensitivities of all the samples were estimated and a sudden increase was observed as the amorphous layer decreased from 225 nm to 90 nm, indicating a transition of creep mechanism in nanolaminates.

Acknowledgement

The support from the National Natural Science Foundation of China (Grant Nos. 11502235, 11672356) and Public Welfare Project of Zhejiang Province (2015C31074) are gratefully acknowledged.

Appendix A. Supplementary data

Supplementary data to this article can be found online at http://dx.doi.org/10.1016/j.jnoncrysol.2017.03.037.

References

[1] C.A. Schuh, T.C. Hufnagel, U. Ramamurty, Acta Mater. 55 (2007) 4067–4109.
[2] N. Nishiyama, K. Takenaka, H. Miura, et al., Intermetallics 30 (2012) 19–24.
[3] S. Pauly, L. Löber, R. Petters, et al., Mater. Today 16 (2013) 37–41.
[4] D.C. Hofmann, J.Y. Suh, A. Wiest, et al., Nature 451 (2008) 1085–1089.
[5] Y. Wang, J. Li, A.V. Hamza, et al., Proc. Natl. Acad. Sci. 104 (2007) 11155–11160.
[6] J.Y. Kim, D. Jang, J.R. Greer, Adv. Funct. Dent. Mater. 21 (2011) 4550–4554.
[7] I. Knorr, N.M. Cordero, E.T. Lilleodden, et al., Acta Mater. 61 (2013) 4984–4995.
[8] Y. Cui, O.T. Abad, F. Wang, et al., Sci. Rep. (2016) 6.
[9] Y. Q. Wang, J. Y. Zhang, X. Q. Liang, et al. Acta. Dent. Mater., 2015 (95) 132–144.
[10] M.C. Liu, J.C. Huang, Y.T. Fong, et al., Acta Mater. 61 (2013) 3304–3313.
[11] J.Y. Zhang, G. Liu, J. Sun, Acta Mater. 66 (2014) 22–31.
[12] W. Guo, E. Jägle, J. Yao, et al., Acta Mater. 80 (2014) 94–106.
[13] W. Guo, E.A. Jägle, P.P. Choi, et al., Phys. Rev. Lett. 113 (2014), 035501. .
[14] I.C. Choi, B.G. Yoo, Y.J. Kim, et al., Nano 5 (2012) 7.
[15] Y. Ma, G.J. Peng, D.H. Wen, et al., Mat. Sci. Eng. A 621 (2015) 111–117.
[16] B.G. Yoo, Y.J. Kim, I.C. Choi, et al., Int. J. Plast. 37 (2012) 108–118.
[17] X.Y. Zhu, X.J. Liu, F. Zeng, et al., Mater. Lett. 64 (2010) 53–56.
[18] H.M. Ledbetter, E.R. Naimon, J. Phys. Chem. Ref. Data 3 (1974) 897–935.
[19] W.D. Nix, Metall. Trans. A. 20 (1989) 2217–2245.
[20] B.E. Schuster, Q. Wei, T.C. Hufnagel, et al., Acta Mater. 56 (2008) 5091–5100.
[21] L. Lu, X. Chen, X. Huang, et al., Science 323 (2009) 607–610.
[22] D. Tabor, Review of Physics in Technology, 1, 1970 145.
[23] H. Guo, P.F. Yan, Y.B. Wang, et al., Nat. Mater. 6 (2007) 735–739.
[24] Y. Ma, G.J. Peng, Y.H. Feng, et al., Mat. Sci. Eng. A 651 (2016) 548–555.
[25] Y. Ma, J.H. Ye, G.J. Peng, et al., Mat. Sci. Eng. A 627 (2015) 153–160.
[26] Y. Ma, Y.H. Feng, T.T. Debela, et al., Int. J. Refract. Met. H 54 (2016) 395–400.
[27] W. Fei, X. Kewei, Mater. Lett. 58 (2004) 2345–2349.
[28] F. Li, Y. Xie, J. Gu, et al., Mat. Sci. Eng. A 648 (2015) 57–60.
[29] S.P. Wen, R.L. Zong, F. Zeng, et al., J. Mater. Res. 22 (2007) 3423–3431.
[30] B. G. Yoo, K. S. Kim, J. H. Oh, et al. Scr. Dent. Mater., 2010 (63) 1205–1208.
[31] J. Hu, G. Sun, X. Zhang, et al., J. Alloys Compd. 647 (2015) 670–680.
[32] Y. Liu, C. Huang, H. Bei, et al., Mater. Lett. 70 (2012) 26–29.
[33] Y. Ma, G.J. Peng, W.F. Jiang, et al., J. Non-Cryst. Solids 442 (2016) 67–72.
[34] Y. Ma, J.H. Ye, G.J. Peng, et al., Mat. Sci. Eng. A 622 (2015) 76–81.
[35] B.G. Yoo, J.H. Oh, Y.J. Kim, et al., Intermetallics, 18, 2010 1898–1901.
[36] A. Bhattacharyya, G. Singh, K.E. Prasad, et al., Mat. Sci. Eng. A 625 (2015) 245–251.
[37] Q. Wei, S. Cheng, K.T. Ramesh, et al., Mat. Sci. Eng. A 381 (2004) 71–79.
[38] K. L. Johnson, Cambridge University Press, UK, 1987.
[39] D. Pan, A. Inoue, T. Sakurai, et al., Proc. Natl. Acad. Sci. 105 (2008) 14769–14772.
[40] D. Tönnies, R. Maaß, C.A. Volkert, Adv. Mater. 26 (2014) 5715–5721.